Thermal Science and Engineering 2025, 8(2), 11631.
https://doi.org/10.24294/tse11631

Article

Thermal behavior investigation on marine reefer container envelopes embedded with vacuum insulation panel

Ankang Kan[1,*,†], Zhaofeng Chen[2,†], Zhiwu Ye[3], Jinsheng Zhang[1], Dan Cao[1], Deng Lu[3], Dong Min[3]

[1] Merchant Marine College, Shanghai Maritime University, Shanghai 201306, China
[2] College of Material Science and Technology, Nanjing University of Aeronautics and Astronautics, Nanjing 210016, China
[3] China Construction Institute of Advanced Technology, Wuhan 430075, China
*** Corresponding author:** Ankang Kan, ankang0537@126.com
[†] These authors are equally contributed.

CITATION

Kan A, Chen Z, Ye Z, et al. Thermal behavior investigation on marine reefer container envelopes embedded with vacuum insulation panel. Thermal Science and Engineering. 2025; 8(2): 11631. https://doi.org/10.24294/tse11631

ARTICLE INFO

Received: 25 March 2025
Accepted: 25 April 2025
Available online: 15 May 2025

Abstract: To investigate the effect of the location of vacuum insulation panels on the thermal insulation performance of marine reefer containers, a 20^{ft} mechanical refrigeration reefer container was employed in this paper, and the physical and mathematical models of three kinds of envelopes composed of vacuum insulation panels (VIP) and polyurethane foam (PU) were numerically established. The heat transfer of three types of envelopes under unsteady conditions was simulated. In order to be able to analyze theoretically, the Rasch transform is used to analyze the thermal inertia magnitude by calculating the thermal transfer response frequency and the thermal transfer response coefficient for each model, and the results are compared with the simulation results. The results implied that the insulation performance of VIP external insulation is the best. The delay times of each model obtained from the simulation results are 0.81 h, 1.45 h, 2.03 h, and 2.24 h, while the attenuation ratios are 8.93, 20.39, 20.62, and 21.78, respectively; the delay times calculated from the theoretical analysis are 0.78 h, 1.43 h, 1.99 h, and 2.20 h, respectively; and the attenuation ratios are 8.84, 20.31, 20.55, and 21.72, respectively. The carbon reduction effect of VIP external insulation is also the best. The most considerable carbon reduction is 3.65894 kg less than the traditional PU structure within 24 h. The research has a guiding significance for the research and progress of the new generation of energy-saving reefer containers and the insulation design of the envelope of refrigerated transportation equipment.

Keywords: vacuum insulation pane; marine reefer container; envelopes; thermal conductivity; energy conservation

1. Introduction

Nowadays, along with the progress of society, science, and technology, food value has been put forward with higher requirements, and refrigerated transportation equipment and technology have been developed [1–3]. Marine reefer containers are employed as multi-transport main equipment for refrigerated cargo on the market. Reefer containers are 7% of the total number of containers. The requirement for reefer containers has a much better increase rate than ordinary containers [4,5]. Refrigeration equipment for reefer containers has been greatly developed [6–8]. However, the scope for improving energy efficiency is extremely limited. To reduce the consumption of sources of energy for reefer containers and carbon emissions, the renovation of their envelopes is the most effective way for refrigerated transportation to improve insulation performance.

Polyurethane foam (PU) material is used as insulation material in traditional

reefer containers, and the thermal conductivity of PU is 0.018–0.032 W/(m·K). Vacuum insulation panels (VIP) are an insulation material with high efficiency, and their thermal conductivity is much lower than traditional insulation materials [9–13]. Because of the strengths of low thermal conductivity, thin thickness, good security, environmental protection, high efficiency, and energy saving. VIP has been extensively employed in refrigerators, cold storage, refrigerated trucks, and other low-temperature refrigerated transportation fields [3,14–16], as well as new energy-saving buildings and other fields with high insulation requirements [9,15,17–19]. Currently, the research on reefer containers mainly focuses on the temperature field distribution inside the container [20–22]. In terms of envelopes [23], they experimentally and numerically investigated a new technique for improving the thermal performance of reefer container envelope structures using phase change materials (PCM). An external PCM layer was integrated with an insulating sandwich panel, and two analyses were performed. Compared to the container, laboratory tests showed that internal wall temperature was reduced with the addition of PCM layers. Outdoor experiments showed that the PCM envelope reduced the rate of heat transfer and obtained the peak delay. Wang et al. [24] explored the thermal performance of the VIP envelope under four design forms with the same coverage of VIP. by means of CFD (computational fluid dynamics), The thermal insulation performance of VIP was affected by polyurethane distribution and the thermal bridge effect. The design form with the least carbon emission and the least thermal bridge effect was found. Although the application of VIP in the thermal insulation envelope of containers is reported, practical engineering application has not yet been found. With the development and maturity of VIP technology [12,25–27], the production scale of VIP will be unprecedentedly expanded, the cost of production will be reduced, and it is potentially applied as a marine reefer container envelope.

This paper is devoted to studying the influence of internal insulation, sandwich insulation, and external insulation of VIP + PU combined as reefer container envelopes, respectively, on the thermal insulation effect of reefer containers under unsteady conditions. In the introduction, the paper proceeds with an in-depth exploration of the topic in a structured manner. The “Structure of VIP” section provides a detailed description of the composition and working principle of VIP. This is crucial as it lays the foundation for understanding how VIPs function within the context of marine reefer container envelopes. The “Simulation method and theoretical calculation method” section is divided into several subparts. It first details the material and model of the marine reefer container, including the dimensions, structure, and different insulation layer configurations. Then, it elaborates on the simulation model, covering aspects such as grid independence verification, governing equations, boundary conditions, and the solution method. The mathematical model subsection presents the reaction coefficient method and the harmonic response method, which are used to analyze the thermal inertia and heat transfer characteristics of the container envelopes. The “Results and discussion” section is where the simulation and theoretical calculation results are presented and analyzed. It includes the simulation results of temperature variation on the internal walls of different containers, calculation results of thermal transfer reaction coefficients and frequencies, as well as an analysis of the energy consumption and emission reduction potential. This section

helps to draw conclusions about the performance of different insulation arrangements. Finally, the "Conclusion" section summarizes the key findings of the study, highlighting the superiority of VIP external insulation in terms of thermal insulation performance and carbon emission reduction.

2. Structure of VIP

2.1. The components of VIP

VIP is a kind of composite material with a special structure, which usually consists of core material, getter, and gas barrier envelopes [28]. Based on the theory of vacuum insulation, gas embodied in the porous core material is removed. When the distance of heat transfer (the aperture of the core material) is less than the molecular average free path of the gas, that is, when the Knudsen number Kn > 10, the heat conduction of the gas will be inhibited [29]. In addition, even at ordinary pressure, for porous core materials with pore size less than 66.5 μm, when the Grashof number Gr < 1000, it indicates that convective heat transfer is negligible. The initial thermal conductivity of VIP mainly depends on the solid thermal conductivity of the core material and the radiation equivalent thermal conductivity [30]. The component of VIP was shown in **Figure 1**.

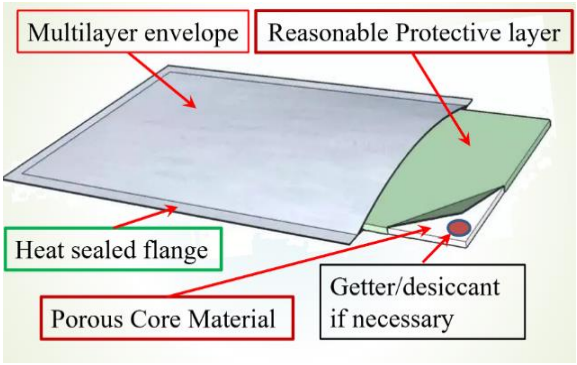

Figure 1. The component of VIP.

2.2. The materials and properties of VIP

Porous materials, such as glass fiber, open-cell organic foam, fumed silica, or a combination of several porous materials, are employed as core materials, which mainly provide structural support to prevent VIP shrinkage and collapse under vacuum, etc. [30]. The gas barrier envelopes are usually made of aluminum-plastic composite film, which is used to provide confined space, maintain the vacuum in the panel, and inhibit heat conduction of residual gas. Its structural characteristic is that the outermost layer is a thermal insulation layer, usually composed of polyethylene terephthalate (PET); the interlayer is the gas barrier layer; and the innermost layer is a heat-sealing layer, which is generally made up of 50–80 μm low-density polyethylene (LDPE) and is bonded between the layers [31]. The effect of the barrier envelope is to vacuum seal the core material, which effectively prevents the outside air and water vapor from penetrating into the VIP to maintain the inner vacuum. The role of the getter is to absorb the residual gas in the VIP and maintain the vacuum in the panel to extend the service life and prolong its excellent insulation performance. The main

performance parameters of VIP and PU were shown in **Table 1** [32].

Table 1. The main performance parameters of VIP and PU.

Performance parameter	VIP	PU
Thermal conductivity	1.0~4.0 mW/(m·K)	18.0~32.0 mW/(m·K)
Compressive strength	0.14~0.25 MPa	0.14~0.2 MPa
Density	220~260 kg/m^3	30~40 kg/m^3
Using temperature	−80~120 ℃	−70~80 ℃
Service life	>15 years	>15 years

Note: Thermal conductivity test conditions: ambient temperature is 25 ℃, relative humidity < RH50%.

3. Simulation method and theoretical calculation method

3.1. Material and model of marine reefer container

The 20^{ft} standard marine reefer container was involved in this paper. The external dimensions of the container were 6058 mm× 2438 mm× 2591 mm (length × width × height), the structure of the reefer container is shown in **Figure 2**.

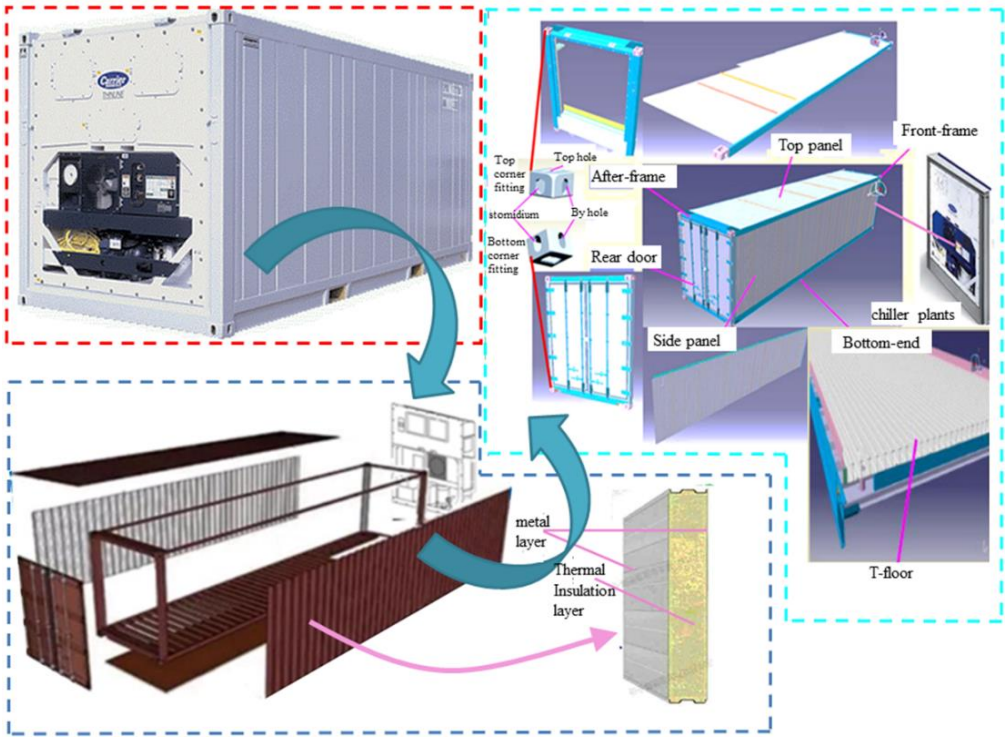

Figure 2. The structure of reefer container.

The envelope of the reefer container was mainly composed of the bottom end, side panel, top panel, front end, after-frame, rear door, etc. On the basis of the relative position of PU and VIP, the envelope was divided into three types: internal insulation (VIP was placed in the inner part of the insulation construction), sandwich insulation (VIP was placed in the middle of the insulation construction), and external insulation (VIP was placed in the outer part of the insulation construction), respectively. The thickness of the thermal insulation layer in different parts of the container and the

physical properties of the main materials were shown in **Tables 2** and **3**.

Table 2. The thickness of the thermal insulation layer in different parts of the container.

Position	The thickness of the VIP δ/(mm)	The thickness of the PU δ/(mm)	The total thickness of the insulation layer δ/(mm)
Side panel (two)	20	42	62
Top panel	20	70	90
Bottom-end	20	53	73
Front-end	/	/	/
Rear door	20	57	77

Table 3. The properties of the main materials.

Material	Thermal conductivity. λ/W/(m^1·K^1)	Specific heat capacity c_p/J/(kg·K)	Density ρ/(kg/m^3)
PU	0.020	1210	30
VIP	0.004	670	120

3.2. Simulation model

3.2.1. Grid independence verification

Softer ware was used to build the models. The hexahedral meshes were established. The temperature was evaluated for 150,000 to 1,400,000 grids in this paper. Grid independence verification was shown in **Figure 3**. From **Figure 3**, when the number of grids was after 700,000, even if the number of grids was increased, the temperature of the internal wall did not change. Therefore, to reduce the computations, 700,000 grid numbers were chosen for numerical calculations.

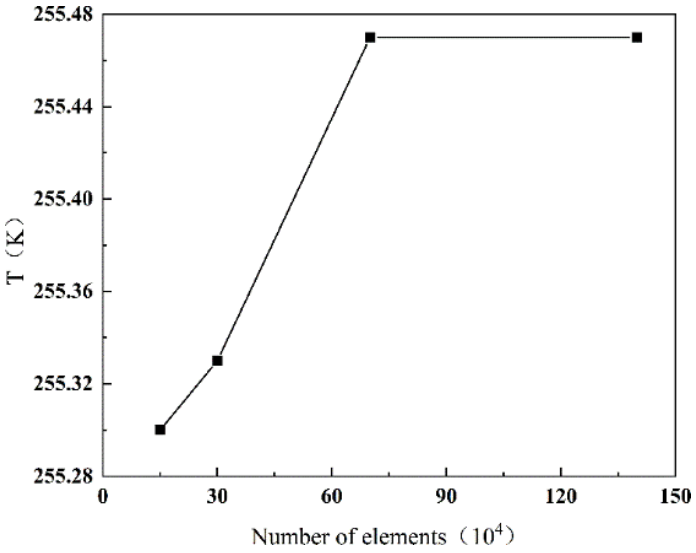

Figure 3. Grid independence verification.

3.2.2. Simulation model and governing equations

Various reefer container models were created and simulated by CFD software in this paper. In order to make close contact between the faces, connecting structural columns are used. The grid model of the container was shown in **Figure 4**. The grid type was hexahedral mesh, which was encrypted in the envelope, and the overall

number of grids was 700,000.

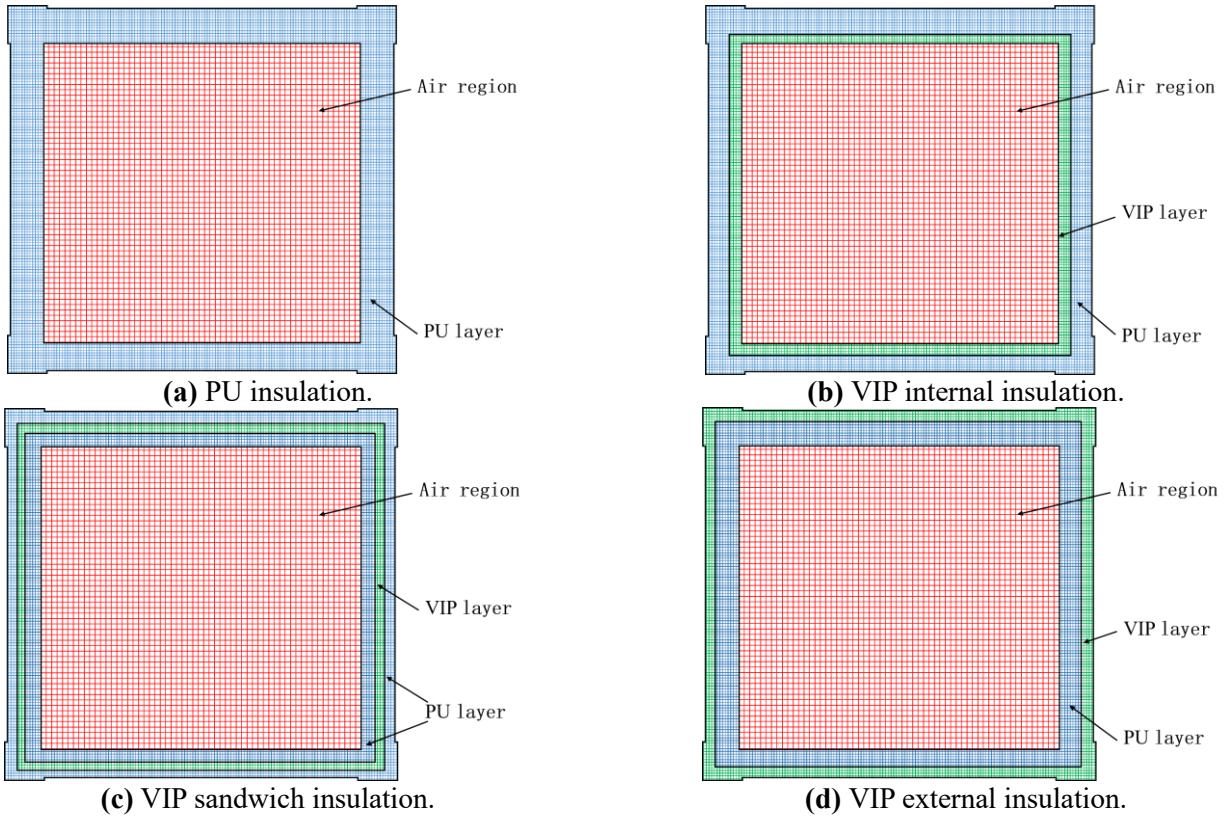

(a) PU insulation. **(b)** VIP internal insulation.

(c) VIP sandwich insulation. **(d)** VIP external insulation.

Figure 4. The grid model of the container.

Based on the real size of the reefer container, the simulated model was established before the 1:1 equal-scale mathematical model was established. For simplification purposes, some essential assumptions were made as the follows:

(1) The layers of materials were in close contact; there was no gap between the layers, and the thermal properties of each layer of material were isotropic and invariant.

(2) The influence of complicated structures in the reefer container was ignored.

(3) There were grilles at the air supply and return ports; the influence of grilles on the supply air and return air was ignored; the size of the air supply outlet was 2314 mm × 30 mm; and the size of the return air inlet was 2314 mm × 130 mm.

(4) The air in the container was Newtonian fluid, which satisfied the Boussinesq hypothesis.

The relevant equations were built, including the mass conservation equation, the momentum conservation equation, and the energy conservation equation:

The mass conservation equation (equation of continuity):

$$\frac{\partial(\rho u)}{\partial x}+\frac{\partial(\rho v)}{\partial y}+\frac{\partial(\rho w)}{\partial z}=0 \tag{1}$$

The momentum conservation equation:

$$X: \quad \frac{u\partial(\rho u)}{\partial x}+\frac{v\partial(\rho u)}{\partial y}+\frac{w\partial(\rho u)}{\partial z}=-\frac{\partial p}{\partial x}+\mu\left(\frac{\partial^2 u}{\partial x^2}+\frac{\partial^2 u}{\partial y^2}+\frac{\partial^2 u}{\partial z^2}\right) \tag{2}$$

$$Y: \quad \frac{u\partial(\rho v)}{\partial x}+\frac{v\partial(\rho v)}{\partial y}+\frac{w\partial(\rho v)}{\partial z}=-\frac{\partial p}{\partial y}+\mu(\frac{\partial^2 v}{\partial x^2}+\frac{\partial^2 v}{\partial y^2}+\frac{\partial^2 v}{\partial z^2}) \quad (3)$$

$$Z: \quad \frac{u\partial(\rho w)}{\partial x}+\frac{v\partial(\rho w)}{\partial y}+\frac{w\partial(\rho w)}{\partial z}=-\frac{\partial p}{\partial z}+\mu(\frac{\partial^2 w}{\partial x^2}+\frac{\partial^2 w}{\partial y^2}+\frac{\partial^2 w}{\partial z^2})-\rho g \quad (4)$$

The energy conservation equation:

$$\frac{u\partial(\rho c_p T)}{\partial x}+\frac{v\partial(\rho c_p T)}{\partial y}+\frac{w\partial(\rho c_p T)}{\partial z}=K(\frac{\partial^2 T}{\partial x^2}+\frac{\partial^2 T}{\partial y^2}+\frac{\partial^2 T}{\partial z^2}) \quad (5)$$

3.2.3. Boundary condition and solution

For the entry boundary conditions, the velocity inlet boundary condition was selected, the outlet velocity was set to 5 m/s, and the supply air temperature was 253 K.

For the outlet boundary conditions, because of the pressure and velocity of the exit, there is indeterminacy. Therefore, the outlet boundary conditions can be regarded as outflow.

The ambient temperature was set as the following fitting function, and the convective heat transfer coefficient was 18.3 W/(m^2·K) [20].

$$t(\tau)=295+4.2\,cos(\frac{\pi}{12}\times\frac{\tau}{3600}) \quad (6)$$

The finite volume method was selected for the solution. The SIMPLE pressure correction algorithm was used, and the pressure model, energy equation, and *k*-*ε* standard equation were used for the solution. The second-order upwind discrete scheme was employed for the advection terms of pressure and temperature. Gravity acceleration *g* was 9.8 m/s^2. The initial temperature was 295 K. The number of calculated steps was 172,800 (48 h), and the calculation time step was 1 s. The temperature variation on the internal face of each container model was recorded simultaneously during the simulation process.

3.3. Mathematical model

For heat transfer, due to the heat storage capacity of the material, when disturbed by transient temperature fluctuations, the temperature field will not change significantly immediately. Instead, it will gradually transition from the disturbed wall to the other wall, and the temperature at each position will slowly change until it is re-stabilized, which reflects the thermal inertia of the material. The thermal inertia index *D* of the envelope is an index reflecting its ability to resist temperature fluctuations and heat flow fluctuations. The larger the value of *D* is, the better the thermal stability of the envelope will be. The thermal inertia index of a single material layer was calculated as [33]:

$$D=RS=\delta\sqrt{\frac{2\pi C_p\rho}{\lambda P}} \quad (7)$$

where *R* was thermal resistance, m^2·K/W; *S* was heat storage coefficient, W/(m^2·K); δ was thickness, m; and *P* was period of fluctuations, s.

The thermal inertia index of the envelope composed of multi-layer materials was calculated as:

$$D = \sum_{i}^{n} D_i \tag{8}$$

3.3.1. Reaction coefficient method

According to Fourier's law of thermal transfer, the governing equation for the thermal transfer process in a one-dimensional single-layer homogeneous envelope was as follows:

$$\frac{\partial t(x,\tau)}{\partial \tau} = a\frac{\partial^2(x,\tau)}{\partial x^2} \tag{9}$$

$$q(x,\tau) = -\lambda\frac{\partial(x,\tau)}{\partial x} \tag{10}$$

The following matrix expressions for the system of algebraic equations can be obtained after applying the Rasch transform method to the spatial variable x and the temporal variable τ of Equations (9) and (10) using the Rasch transform method.

$$\begin{bmatrix} T(l,s) \\ Q(l,s) \end{bmatrix} = \begin{bmatrix} 1 & -\frac{1}{h_{in}} \\ 0 & 1 \end{bmatrix} \begin{bmatrix} ch(\sqrt{\frac{s}{a}}l) & -\frac{sh(\sqrt{\frac{s}{a}}l)}{\lambda\sqrt{\frac{s}{a}}} \\ -\lambda\sqrt{\frac{s}{a}}sh(\sqrt{\frac{s}{a}}l) & ch(\sqrt{\frac{s}{a}}l) \end{bmatrix} \begin{bmatrix} 1 & -\frac{1}{h_{out}} \\ 0 & 1 \end{bmatrix} \begin{bmatrix} T(0,s) \\ Q(0,s) \end{bmatrix} \tag{11}$$

The second square on the right side of the equation is independent of the input and output parameters of the envelope, i.e., it is independent of the temperature and thermal flow on both sides of the envelope and represents only the thermal properties of the single-layer homogeneous envelope itself [34], as shown in Equation (12).

$$[G_i] = \begin{bmatrix} A_i(s) & -B_i(s) \\ -C_i(s) & D_i(s) \end{bmatrix} \tag{12}$$

The matrix expression for the system of algebraic equations obtained after the Rasch transformations of the multilayer envelope is given in Equation (13).

$$\begin{bmatrix} T(l,s) \\ Q(l,s) \end{bmatrix} = \begin{bmatrix} 1 & -\frac{1}{h_{in}} \\ 0 & 1 \end{bmatrix} [G_n][G_{n-1}]\cdots[G_1] \begin{bmatrix} 1 & -\frac{1}{h_{out}} \\ 0 & 1 \end{bmatrix} \begin{bmatrix} T(0,s) \\ Q(0,s) \end{bmatrix} \tag{13}$$

The basic steps in theoretically solving for the thermal transfer response coefficient $Y(j)$ for a multilayer envelope are summarized below:

(1) Construct the transfer matrix of the multilayer envelope after the Rasch transformation and simplify it to a single matrix, as shown in Equation (14);

$$\begin{bmatrix} A(s) & -B(s) \\ -C(s) & D(s) \end{bmatrix} = \begin{bmatrix} 1 & -\frac{1}{h_{in}} \\ 0 & 1 \end{bmatrix} [G_n][G_{n-1}]\cdots[G_n] \begin{bmatrix} 1 & -\frac{1}{h_{out}} \\ 0 & 1 \end{bmatrix} \tag{14}$$

(2) Solve for the value of the roots of the transcendental equation $B(s) = 0$,α_i;

(3) Solve for the coefficients β_i of the Laplace inverse transform, as shown in Equation (15);

$$\beta_i = -\frac{1}{s^2 B'(s)}\Big|_{s=-\alpha_i} \tag{15}$$

(4) The discrete heat transfer response coefficients $Y(j)$ of the multilayer envelope can be calculated by substituting α_i, β_i into the following two Equations (16) and (17).

$$Y(0) = K_1 + \sum_{i=1}^{\infty} \frac{\beta_i}{\Delta\tau}(1 - e^{-\alpha_i \Delta\tau}) \qquad j = 0 \tag{16}$$

$$Y(j) = -\sum_{i=1}^{\infty} \frac{\beta_i}{\Delta\tau}(1 - e^{-\alpha_i \Delta\tau})\ {}^{2}e^{-(j-1)\alpha_i \Delta\tau} \qquad j \geq 1 \tag{17}$$

3.3.2. Harmonic response method

The harmonic response method is commonly used to analyze the thermal transfer response frequency of multilayer envelopes. The frequency of the thermal transfer response is mainly represented by two parameters, the delay time and the attenuation ratio, the magnitude of which can reflect the thermal inertia of the structure to a certain extent [35–37]. The attenuation ratio and delay time need to be solved separately for each envelope depending on its composition and thermophysical properties.

$$v = 0.9e^{\frac{\sum D}{\sqrt{2}}} \frac{S_1 + h_{in}}{S_1 + Y_1} \frac{S_2 + Y_1}{S_2 + Y_2} \cdots \frac{S_n + Y_{n-1}}{S_n + Y_n} \frac{Y_n + h_{out}}{h_{out}} \tag{18}$$

$$\Delta t = \frac{1}{15}(40.5 \sum D - arctan \frac{h_{in}}{h_{in} + \sqrt{2}Y_i} + arctan \frac{Y_e}{Y_e + \sqrt{2}h_{out}}) \tag{19}$$

D = 1 is used as a standard of judgment to determine the surface thermal storage coefficient. Y_i calculated the surface thermal storage coefficient of the material layer from the direction of the advancing counter-temperature wave and then extrapolated layer by layer to the surface of the temperature wave facing the wave. Use the internal side material layer as the first layer.

D = 1 is used as a standard of judgment to determine Y_i, calculation of Y_i of the material layer is calculated from the direction of the advancing counter-temperature wave, and then extrapolated layer by layer to the surface of the temperature wave facing the wave. Use the internal side material layer as the first layer:

(1) If the thermal inertia index of the first layer material $D_1 \geq 1, Y_i = D_1$;

(2) If the thermal inertia index of the previous j-layer material $\sum D_j \geq 1, \sum D_{j-1}$, then the internal surface thermal storage coefficient of the j-th layer of material $Y_j = S_j$, calculate the thermal storage coefficient of the internal surface of the $j-1$ layer of the material Y_{j-1}, then the thermal storage coefficients for the $j-2$ and $j-3$ layers Y_{j-2}, Y_{j-3} are calculated in turn; finally solve for the thermal storage coefficient of layer 1st Y_1. At this point, the thermal storage coefficient of the first layer of material is the thermal storage coefficient of the internal surface of the

envelope, i.e., $Y_i = Y_1$. The equations are shown in Equations (20–22);

$$Y_{j-1} = \frac{R_{j-1}S_{j-1}^2 + Y_j}{1 + R_{j-1}Y_j} \tag{20}$$

$$Y_{j-2} = \frac{R_{j-2}S_{j-2}^2 + Y_{j-1}}{1 + R_{j-2}Y_{j-1}} \tag{21}$$

$$Y_i = Y_1 = \frac{R_1S_1^2 + Y_2}{1 + R_1Y_2} \tag{22}$$

(1) If the thermal inertia index of the material as a whole is $D < 1$, the calculation of the thermal storage coefficient of the most external layer of the material is carried out directly:

$$Y_n = \frac{R_nS_n^2 + h_{out}}{1 + h_{out}} \tag{23}$$

where R_n is the most external layer envelope thermal resistance, (m^2·K)/W, S_n is the thermal storage coefficient of the layer material, W/(m^2·K), α_{out} is the convective coefficient of thermal exchange of the external surface of the envelope, W/(m^2·K).

4. Results and discussion

4.1. Simulation results

The results of temperature variation on the internal walls of different containers were shown in **Figure 5**. It was found that with the fluctuation of the temperature of the outer wall, the temperature of the internal wall also fluctuated. In the initial stage, the cold energy was transferred from inside to outside through the internal air region, and the temperature of the internal wall gradually decreased until the wall dissipation rate and the release rate of cold energy reached a dynamic balance.

From the data after the first equilibrium point (the first extreme point of the temperature curve), it can be seen that the external temperature curve and internal wall temperature curve of each model were not synchronized in time, i.e., there was a phase difference, which was named the delay time. Moreover, the temperature fluctuation range was also different, and the ratio of the fluctuation range of the two was named the attenuation ratio. Two extreme points adjacent to each other on the inner wall temperature curve were selected to calculate the delay time and attenuation ratio. After calculation, the delay time of the four containers was 0.8 h, 1.4 h, 2.0 h, and 2.2 h successively, while the attenuation magnification was 8.93, 20.39, 20.62, and 21.78 successively. The thermal inertia index, delay time, and attenuation ratio of each container model were shown in **Table 4**.

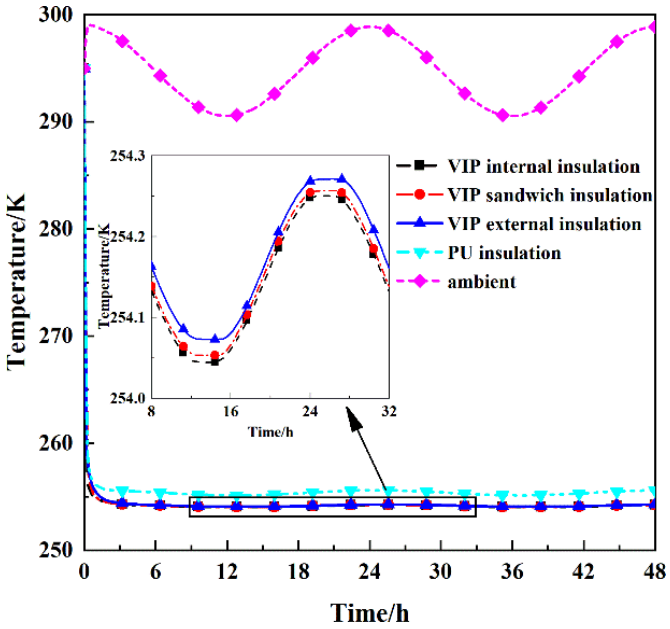

Figure 5. The temperature variation on the internal walls of different containers.

Table 4. The thermal inertia index, delay time, and attenuation ratio of each container model.

Insulation method	The thermal inertia index	Delay time/h	Attenuation ratio
PU insulation	4.71	0.8	8.93
VIP internal insulation	4.79	1.45	20.39
VIP sandwich insulation	4.84	2.03	20.62
VIP external insulation	5.44	2.24	21.78

The calculation results show that the thermal inertness index of the container with the VIP external thermal insulation arrangement was larger, and its resistance to external disturbance temperature waves was stronger. In this case, the temperature range of the internal wall was smaller, which was conducive to maintaining a stable internal ambient air temperature. Therefore, the use of VIP external thermal insulation was conducive to the stability of the temperature of the inner wall of the container, and the thermal inertia was maximum.

On the other hand, the cross-section of the temperature field of each model envelope was shown in **Figure 6** when the calculation reached 86,400 steps (i.e., 24 h after the temperature change). It can be seen that there was an obvious temperature gradient at the VIP position. It indicated that the VIP blocking effect on temperature diffusion was stronger, the influence of external temperature disturbance on the temperature field inside the VIP was weaker, the temperature disturbance of the insulation layer inside the VIP was smaller, and the thermal compensation of the internal air reign was more adequate, the internal ambient temperature was more stable.

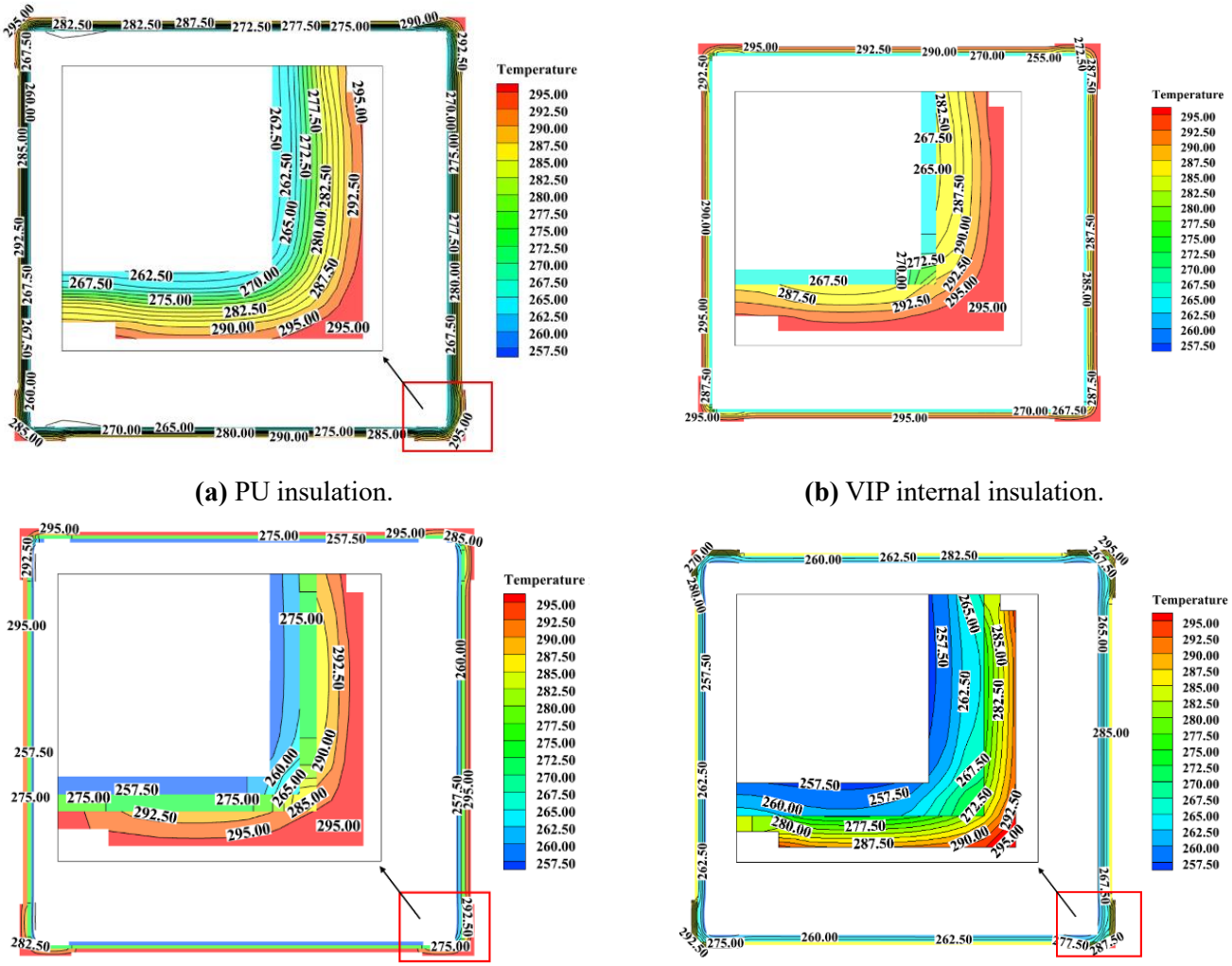

(a) PU insulation. **(b)** VIP internal insulation.

(c) VIP sandwich insulation. **(d)** VIP external insulation.

Figure 6. The temperature field of the container model.

4.2. Numerical calculation and discussion

4.2.1. Calculation results of thermal transfer reaction coefficient

The thermal transfer reaction coefficient is a sum of infinite indices related to the zero-value solutions of the $B(s)$ elements in the transfer matrix, but there are infinitely many zero-value solutions of the $B(s)$ elements, and it is obviously impossible to find out all of them. Generally, only the solutions larger than −40 can meet the accuracy requirement. The results of the solution using MATLAB are shown in **Table 5**.

Table 5. Thermal transfer response coefficients for each container model.

Insulation method	0 h	1 h	2 h	3 h	4 h
PU insulation	0.2812	0.5947	0.0793	0.0106	0.0014
VIP internal insulation	0.1758	0.3536	0.0589	0.0131	0.0029
VIP sandwich insulation	0.1626	0.3251	0.0772	0.0161	0.0036
VIP external insulation	0.1345	0.2824	0.0941	0.0314	0.0105

It can be seen that when a unit temperature disturbance is applied to the wall, the thermal response coefficients of each model show a tendency to increase and then decrease. It can be seen that the time-to-time thermal conductivity of the internal wall surface is a process from weak to strong and then to weak. In particular, at 1 h, the hourly heat transfer of the VIP inner insulation container is the largest, followed by the sandwich insulation, and the outer insulation is the lowest. At other moments, the hourly thermal transfer of the VIP external insulation container is the highest, followed by the sandwich insulation, and the lowest by the internal insulation. This characteristic shows that, under the same influence of temperature disturbance, the time-to-time heat transfer on the internal wall surface of the internal insulated container is more drastic, whereas the external insulated container is relatively smooth. In a practical sense, when VIP adopts the arrangement of external insulation, it can make the multi-layer envelope have more stable thermal compensation and help to keep the internal ambient temperature relatively stable.

4.2.2. Calculation results of thermal transfer response frequency

The delay times and attenuation ratios for each model are shown in **Table 6**.

Table 6. Thermal transfer response frequencies for each container model.

Insulation method	Delay time/h	Attenuation ratio
PU insulation	0.78	8.84
VIP internal insulation	1.43	20.31
VIP sandwich insulation	1.99	20.55
VIP external insulation	2.20	21.72

The above results are compared with the simulation results, and the results are shown in **Table 7**.

Table 7. Thermal transfer response frequencies for each container model under different research methods.

	Simulation results		Theoretical analysis results	
	Delay time/h	Attenuation ratio	Delay time/h	Attenuation ratio
PU insulation	0.81	8.93	0.78	8.84
VIP internal insulation	1.45	20.39	1.43	20.31
VIP sandwich insulation	2.03	20.62	1.99	20.55
VIP external insulation	2.24	21.78	2.20	21.72

The above results are analyzed theoretically. Because the change of temperature field is related to the diffusion of the disturbing temperature wave, and the diffusion of the temperature wave is related to the diffusion of the heat flow wave. Under the unsteady condition, the difference in insulation effect caused by the arrangement order of the multi-layer envelope structure is closely relevant to the intensity of temperature disturbance and the thermal properties of each material. When one side of the envelope is disturbed by a temperature perturbation, the thermal insulation layers in the multi-layer envelope are affected successively. After the temperature disturbance passes through the previous layer of insulation, its disturbance strength will have different

degrees of attenuation, and the degree of attenuation is relevant to the thermal inertia of the material itself, and the greater the thermal inertia, the greater the degree of attenuation.

In this study, for the external thermal insulation container, the VIP position is close to the outdoor air side, which is subject to strong temperature disturbance. When the heat flow wave passes through the VIP layer, it will have a significant weakening effect. Therefore, the PU layer inside the VIP layer will be subjected to smaller heat flow disturbance. In the case of a smaller heat flow disturbance, its temperature field changes more slowly. At this time, the multi-layer envelope can provide more thermal compensation to the internal environment, so its thermal stability is better.

4.3. Energy consumption and emission reduction potential

The calculation method for carbon emissions was as follows:

$$\text{Emissions} = \text{AD} \times \text{EF} \tag{24}$$

where emission was greenhouse gas emissions (t); AD was activity level data (heat consumption, GJ); and EF was emission factor (0.11 t CO_2/GJ). Therefore, the heat transfer and reduced carbon emissions of different containers were shown in **Figure 7**.

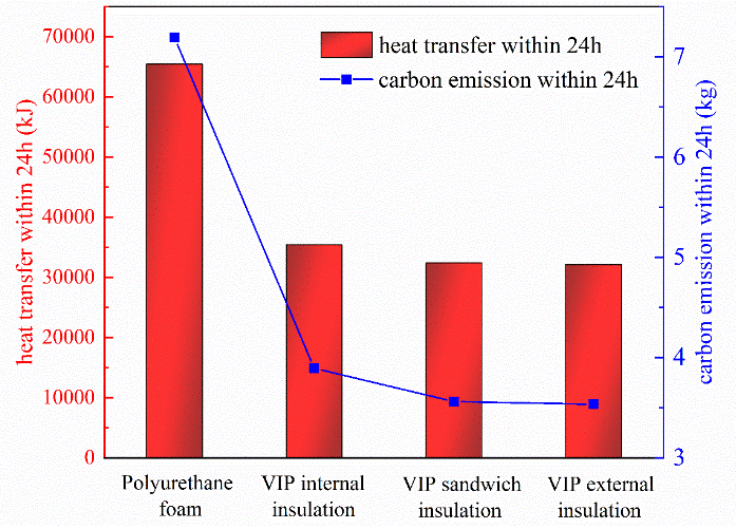

Figure 7. The heat transfer and reduced carbon emissions of different containers.

From **Figure 7**, within 24 h, the heat transfer of the PU thermal insulation container was 65,384.1 kJ, the heat transfer of the VIP thermal insulation container was 35,388.5 kJ, the heat transfer of the VIP sandwich thermal insulation container was 32,368.2 kJ, and the heat transfer of the VIP external thermal insulation container was 32,121.0 kJ. The carbon emission of the PU insulation container was 7.19225 kg, the carbon emission of the VIP insulation container was 3.89274 kg, the carbon emission of the VIP sandwich insulation container was 3.56050 kg, and the carbon emission of the VIP external insulation container was 3.53331 kg. The carbon emission of the VIP external thermal insulation was the minimum among the four types, which was 3.65894 kg, less than that of PU insulation within 24 h. Therefore, VIP external insulation was more conducive to energy saving and emission reduction,

and reefer container envelope insulation using VIP external insulation was the best.

5. Conclusion

The influence of VIP installed in different positions of the container envelope on the thermal insulation performance was studied in this paper. By constructing four kinds of reefer container models, the insulation construction of the container was PU, VIP in the inner of PU, VIP in the middle of PU, and VIP in the outer of PU, respectively. The CFD method was used to simulate. The thermal insulation performance and carbon emission reduction of each container model were compared. The conclusions are as follows:

The envelope of the reefer container with VIP external insulation had the most considerable attenuation and delay effect on external temperature disturbance, the temperature variation of the multi-layer insulation construction was the smallest, the overall thermal stability was the best, and the thermal inertia was the best. The delay times of each model obtained from the simulation results are 0.81 h, 1.45 h, 2.03 h, and 2.24 h, while the attenuation ratios are 8.93, 20.39, 20.62, and 21.78, respectively; the delay times calculated from the theoretical analysis are 0.78 h, 1.43 h, 1.99 h, and 2.20 h, respectively; and the attenuation ratios are 8.84, 20.31, 20.55, and 21.72, respectively. The carbon reduction effect of the reefer container with VIP external insulation was also the best, 3.65894 kg less than that of PU insulation within 24 h. The energy-saving and carbon-reduction effect was obviously the best one.

Taking the cost into consideration, it is currently a significant factor affecting their widespread application in marine reefer containers. Although the production scale of VIPs is expected to expand with the development of technology, reducing production costs, at present, they are more expensive than traditional polyurethane foam (PU). However, considering the long-term energy-saving benefits of VIPs, the reduced energy consumption and carbon emissions can offset part of the higher initial investment. What is more, marine environments are harsh, with high humidity, saltwater corrosion, and mechanical vibrations. The gas barrier envelopes of VIPs are usually made of aluminum-plastic composite film. While this material can maintain the vacuum inside the panel, it may be vulnerable to damage from saltwater corrosion and mechanical stress during long-term use in marine containers. Future research could focus on advanced gas barrier materials. Additionally, proper maintenance and inspection procedures need to be established to ensure the integrity of VIPs during their service life in marine reefer containers.

Author contributions: Conceptualization, AK and ZC; methodology, AK; software, JZ; validation, DL, DM and ZY; formal analysis, DC; investigation, AK; resources, ZC; writing—original draft preparation, AK and JZ; writing—review and editing, DC; supervision, ZC; project administration, AK and ZC; funding acquisition, DL, DM and ZY. All authors have read and agreed to the published version of the manuscript.

Institutional review board statement: Not applicable.

Informed consent statement: Not applicable.

Conflict of interest: The authors declare no conflict of interest.

Nomenclature

λ	thermal conductivity (W/(m·K))	μ	Dynamic viscosity of air (kPa·s)
u	X-axial velocity component (m/s)	v	Y-axial velocity component (m/s)
w	Z-axial velocity component (m/s)	p	Pressure (Pa)
g	Gravity acceleration (m/s)	T	Temperature (K)
K	Heat transfer coefficient (W/(m^2·K^1))	ρ	Density (kg/m^3)
c_p	Specific heat capacity at constant pressure (J/(kg·K))		

References

1. Qi T, Ji J, Zhang X, et al. Research progress of cold chain transport technology for storage fruits and vegetables. Journal of Energy Storage. 2022; 56: 105958. doi: 10.1016/j.est.2022.105958
2. Zhao H, Liu S, Tian C, et al. An overview of current status of cold chain in China. International Journal of Refrigeration. 2018; 88: 483-495. doi: 10.1016/j.ijrefrig.2018.02.024
3. Zhao R, Qiao L, Gao Z, et al. Effect of vacuum insulation panels on energy consumption and thermal load transfer between compartments in a three-temperature frost-free refrigerator. Energies. 2020; 13(7): 1559. doi: 10.3390/en13071559
4. Castelein B, Geerlings H, Van Duin R. The reefer container market and academic research: A review study. Journal of Cleaner Production. 2020; 256: 120654. doi: 10.1016/j.jclepro.2020.120654
5. Meng X, Sun J, Wang H. Cost Analysis of Multimodal Transport on Refrigerated Container. IOP Conference Series: Earth and Environmental Science. 2021; 791(1): 012078. doi: 10.1088/1755-1315/791/1/012078
6. Ozsipahi M, Kose HA, Kerpicci H, et al. Experimental study of R290/R600a mixtures in vapor compression refrigeration system. International Journal of Refrigeration. 2022; 133: 247-258. doi: 10.1016/j.ijrefrig.2021.10.004
7. Tao Y, Hwang Y, Radermacher R, et al. Experimental study on electrochemical compression of ammonia and carbon dioxide for vapor compression refrigeration system. International Journal of Refrigeration. 2019; 104: 180-188. doi: 10.1016/j.ijrefrig.2019.05.009
8. Yang Y, Zhu Y, Zhang Z, et al. Experimental study on performance of double-mode refrigeration system. Applied Thermal Engineering. 2021; 188: 116670. doi: 10.1016/j.applthermaleng.2021.116670
9. Fantucci S, Garbaccio S, Lorenzati A, et al. Thermo-economic analysis of building energy retrofits using VIP - Vacuum Insulation Panels. Energy and Buildings. 2019; 196: 269-279. doi: 10.1016/j.enbuild.2019.05.019
10. Hasanzadeh R, Azdast T, Lee PC, et al. A review of the state-of-the-art on thermal insulation performance of polymeric foams. Thermal Science and Engineering Progress. 2023; 41: 101808. doi: 10.1016/j.tsep.2023.101808
11. V.C., M., S., S., B., P., et al. Preparation, characterisation and thermal property study of micro/nanocellulose crystals for vacuum insulation panel application. Thermal Science and Engineering Progress. 2021; 25: 101045. doi: 10.1016/j.tsep.2021.101045
12. Zach J, Novák V. Polymer-matrix-bonded polyester fibers as a substitute for materials used for the cores of vacuum insulation panels. Materiali in tehnologije. 2019; 53(4): 511-514. doi: 10.17222/mit.2018.208
13. Zach J, Peterková J, Dufek Z, et al. Development of vacuum insulating panels (VIP) with non-traditional core materials. Energy and Buildings. 2019; 199: 12-19. doi: 10.1016/j.enbuild.2019.06.026
14. Gaedtke M, Wachter S, Kunkel S, et al. Numerical study on the application of vacuum insulation panels and a latent heat storage for refrigerated vehicles with a large Eddy lattice Boltzmann method. Heat and Mass Transfer. 2019; 56(4): 1189-1201. doi: 10.1007/s00231-019-02753-4
15. Biswas K, Patel T, Shrestha S, et al. Whole building retrofit using vacuum insulation panels and energy performance analysis. Energy and Buildings. 2019; 203: 109430. doi: 10.1016/j.enbuild.2019.109430
16. Verma S, Singh H. Vacuum insulation panels for refrigerators. International Journal of Refrigeration. 2020; 112: 215-228. doi: 10.1016/j.ijrefrig.2019.12.007
17. Alam M, Picco M, Resalati S. Comparative holistic assessment of using vacuum insulated panels for energy retrofit of office buildings. Building and Environment. 2022; 214: 108934. doi: 10.1016/j.buildenv.2022.108934

18. Geng Y, Han X, Zhang H, et al. Optimization and cost analysis of thickness of vacuum insulation panel for structural insulating panel buildings in cold climates. Journal of Building Engineering. 2021; 33: 101853. doi: 10.1016/j.jobe.2020.101853
19. Uriarte A, Garai I, Ferdinando A, et al. Vacuum insulation panels in construction solutions for energy efficient retrofitting of buildings. Two case studies in Spain and Sweden. Energy and Buildings. 2019; 197: 131-139. doi: 10.1016/j.enbuild.2019.05.039
20. Kan A, Wang T, Zhu W, et al. The characteristics of cargo temperature rising in reefer container under refrigeration-failure condition. International Journal of Refrigeration. 2021; 123: 1-8. doi: 10.1016/j.ijrefrig.2020.12.007
21. Senguttuvan S, Youn JS, Park J, et al. Enhanced airflow in a refrigerated container by improving the refrigeration unit design. International Journal of Refrigeration. 2020; 120: 460-473. doi: 10.1016/j.ijrefrig.2020.08.019
22. Tong Y, Yang H, Bao L, et al. Analysis of Thermal Insulation Thickness for a Container House in the Yanqing Zone of the Beijing 2022 Olympic and Paralympic Winter Games. International Journal of Environmental Research and Public Health. 2022; 19(24): 16417. doi: 10.3390/ijerph192416417
23. Fioretti R, Principi P, Copertaro B. A refrigerated container envelope with a PCM (Phase Change Material) layer: Experimental and theoretical investigation in a representative town in Central Italy. Energy Conversion and Management. 2016; 122: 131-141. doi: 10.1016/j.enconman.2016.05.071
24. Wang J, Ma X, Sun Y, et al. Thermal performance and sustainability assessment of refrigerated container with vacuum insulation panel envelope layer at different design forms. Thermal Science and Engineering Progress. 2023; 42: 101928. doi: 10.1016/j.tsep.2023.101928
25. Kaufmann P, Mai F, Baars S, et al. Develop a multifunctional interior wall insulation material using high-damping, thin and innovative VIP glass fiber (German). Bauphysik. 2020; 42(2): 73-85. doi: 10.1002/bapi.202000002
26. Mao S, Kan A, Zhu W, et al. The impact of vacuum degree and barrier envelope on thermal property and service life of vacuum insulation panels. Energy and Buildings. 2020; 209: 109699. doi: 10.1016/j.enbuild.2019.109699
27. Zheng QR, Zhu ZW, Chen J, et al. Preparation of carbon based getter for glass fiber core vacuum insulation panels (VIPs) used on marine reefer containers. Vacuum. 2017; 146: 111-119. doi: 10.1016/j.vacuum.2017.09.040
28. Kan A, Zhang X, Chen Z, et al. Effective thermal conductivity of vacuum insulation panels prepared with recyclable fibrous cotton core. International Journal of Thermal Sciences. 2023; 187: 108176. doi: 10.1016/j.ijthermalsci.2023.108176
29. König J, Nemanič V, Žumer M, et al. Evaluation of the contributions to the effective thermal conductivity of an open-porous-type foamed glass. Construction and Building Materials. 2019; 214: 337-343. doi: 10.1016/j.conbuildmat.2019.04.109
30. Di X, Xie Z, Chen J, et al. Residual gas analysis in vacuum insulation panel (VIP) with glass fiber core and investigation of getter for VIP. Building and Environment. 2020; 186: 107337. doi: 10.1016/j.buildenv.2020.107337
31. Zhao W, Yan W, Zhang Z, et al. Development and performance evaluation of wood-pulp/glass fibre hybrid composites as core materials for vacuum insulation panels. Journal of Cleaner Production. 2022; 357: 131957. doi: 10.1016/j.jclepro.2022.131957
32. Aditya L, Mahlia TMI, Rismanchi B, et al. A review on insulation materials for energy conservation in buildings. Renewable and Sustainable Energy Reviews. 2017; 73: 1352-1365. doi: 10.1016/j.rser.2017.02.034
33. Xiao M, Zhang GQ. The Influence of Thermal Inertia Index on the Residential External Walls in Hot-Summer and Cold-Winter Areas. Applied Mechanics and Materials. 2013; 368-370: 562-565. doi: 10.4028/www.scientific.net/amm.368-370.562
34. Zhao Y, Zhang X, Xu X. Application and research progress of cold storage technology in cold chain transportation and distribution. Journal of Thermal Analysis and Calorimetry. 2019; 139(2): 1419-1434. doi: 10.1007/s10973-019-08400-8
35. Kan A, Zheng N, Zhu W, et al. Innovation and development of vacuum insulation panels in China: A state-of-the-art review. Journal of Building Engineering. 2022; 48: 103937. doi: 10.1016/j.jobe.2021.103937
36. Fantucci S, Garbaccio S, Lorenzati A, et al. Thermo-economic analysis of building energy retrofits using VIP - Vacuum Insulation Panels. Energy and Buildings. 2019; 196: 269-279. doi: 10.1016/j.enbuild.2019.05.019
37. Thiessen S, Knabben FT, Melo C, et al. A study on the effectiveness of applying vacuum insulation panels in domestic refrigerators. International Journal of Refrigeration. 2018; 96: 10-16. doi: 10.1016/j.ijrefrig.2018.09.006